JOURNAL OF AIRCRAFT
Vol. 45, No. 1, January–February 2008

Transition Point Detection from the Surface Pressure Distribution for Controller Design

Andrei Vladimir Popov,* Ruxandra Mihaela Botez,† and Michel Labib‡
École de Technologie Supérieure, Montréal, Quebec H3C 1K3 Canada

DOI: 10.2514/1.31488

A method for the detection of the location of laminar-to-turbulent transition on the suction surface of an airfoil from the surface pressure distribution is examined. The location of transition is determined for two reference laminar airfoil types: NACA 4415 and WTEA-TE1, as well as for 17 modified WTEA-TE1 airfoil shapes, obtained by displacing the flexible wing upper surface using a single point control mechanism. The second derivative of the pressure distribution is calculated, using two interpolation schemes: piecewise cubic Hermite interpolating polynomial and Spline, from which it is determined that transition may be identified as the location of maximum curvature in the pressure distribution. The results of this method are validated using the well-known XFoil code, which is used to theoretically calculate the transition point position. Advantages of this new method in the real-time control of the location of the transition point are presented.

Nomenclature

C_p	=	pressure coefficient $=(p - p_\infty/q_\infty)$ $=(p - p_\infty/0.5\rho U_\infty)$
c	=	airfoil chord
M	=	Mach number
p	=	static pressure
q	=	dynamic pressure
Re	=	Reynolds number
U_∞	=	freestream velocity
x	=	streamwise distance from airfoil leading edge
α	=	angle of attack
ρ	=	air density

Subscript

∞	=	freestream

I. Introduction

THE modern era of aviation opened a new horizon of research in the morphing adaptive wing concept, encouraged by rising fuel costs and environmental concerns. Adaptive wings, which have the potential to revolutionize the aerospace industry and would be highly beneficial from both commercial and military standpoints, target the enhancement of airfoil efficiency in off-design regimes via drag reduction and lift augmentation, leading to improvements in aircraft performance. Adaptive wing technology may be implemented on mainly two different scales: 1) the large scale through the use of flaps, spoilers, ailerons, etc. and 2) the small scale through boundary-layer control. Although the prospect of cost effectively designing commercial and/or military vehicles with extensive adaptive wing technology may be unlikely in the immediate future, various research into adaptive technology at both the small and large scales are being conducted, especially in the area of boundary-layer control [1].

Several authors have studied this concept from both theoretical and experimental perspectives, and several airfoil shape optimization techniques have been developed; however, implementation into an aircraft structure has yet to be considered [1–3]. The main objective of this type of control is to reduce drag by modifying the location of the laminar-to-turbulent flow transition point on the wing upper surface for a range of operating flow conditions characterized by the Mach number, Reynolds number, and angle of attack. The in-flight modification of aircraft wings can be done to maintain laminar flow over the wing surface as flight conditions change, which will reduce drag and therefore fuel consumption.

Although advances have been made in the development of laminar flow airfoils, there are several problems which require careful attention if further improvements are to be realized in the development of a wing with laminar flow over a large portion of its surface. One important concern is the formation and behavior of the laminar separation bubble, predominantly present at low Reynolds numbers, which plays an important part in determining the character of the boundary layer and the stall characteristics of the airfoil. Studies of the separation of the laminar boundary layer, ensuing transition of the separated shear layer, and the subsequent reattachment and redevelopment of the turbulent boundary layer have already been realized to predict and understand this complex flow phenomenon from both theoretical [4–6] as well as experimental [7] standpoints. An excellent tool is the XFoil free-licensed software which is a boundary-layer solver developed by Drela [8,9]. This software implements the e^N method for transition point detection coupled with a viscous/inviscid flow panel-method solver. The optimal airfoil shapes were represented with a parameterized curve equation, allowing the system to learn the map from the flight-condition parameter values to the curve parameter values [1].

A complex system, however, would adjust the airfoil shape based on the location of the transition point determined from the measured surface pressure distribution. As seen in Fig. 1, for various airfoil types and flow conditions (angles of attack α, speeds V, and Reynolds numbers Re), the controller would receive the airfoil upper surface C_p distributions from the optical sensors, compare it to a computational fluid dynamics (CFD) generated database in which transition points will be given for various airfoil types as a function of the C_p distribution, and determine the transition point once a match is found. The controller would subsequently analyze the transition point position and modify the airfoil shape accordingly using memory alloy actuators for real-time variable flow conditions. The overall aim of the controller will be to reduce the drag force on the

Received 16 April 2007; revision received 13 July 2007; accepted for publication 16 July 2007.

*Ph.D. Student, Automated Production Engineering, Laboratory of Research in Active Controls, Aeroservoelasticity and Avionics, 1100 Notre Dame West.

†Professor, Automated Production Engineering, Laboratory of Research in Active Controls, Aeroservoelasticity and Avionics, 1100 Notre Dame West.

‡M.S. Student, Automated Production Engineering, Laboratory of Research in Active Controls, Aeroservoelasticity and Avionics, 1100 Notre Dame West.

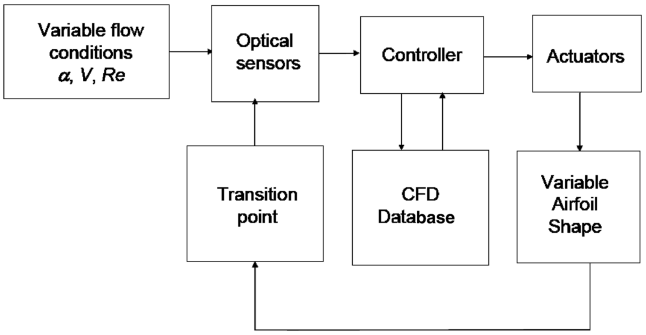

Fig. 1 Closed-loop flow control (with optical sensors and feedback) of the morphing wing design in a wind tunnel.

airfoil upper surface in the vicinity of the trailing edge, given the same set of airflow conditions (angle of attack, airspeed, and Reynolds number) and the same lift force, through changes in the transition point position.

The work presented in this paper is concerned with only a small part of the closed-loop flow control design shown in Fig. 1. Focus was placed on the relationship between the transition point positions provided by the CFD database and the chordwise pressure coefficient distributions.

This relationship will be extremely helpful in real-time controller future design because it will allow for the detection of the transition point position on modified intermediate airfoil shapes only from experimental pressure coefficient distributions. The main advantage of this work is that controller design and real-time simulation of the entire system will therefore be easier to implement.

II. Experimental Setup

The wind tunnel to be used for this experiment is the NRC–IAR (National Research Council—Institute for Aeronautical Research) 2 m × 3 m subsonic wind tunnel, which has a maximum airspeed of 140 m/s ($M = 0.41$) and a turbulence level of 0.16%. The design properties of the wing model are the wing trailing edge airfoil (WTEA) shape, a chord of 0.5 m and a span of 1.2 m. The WTEA is an airfoil optimized for laminar flow in transonic speed (Mach between 0.75–0.8) but due to the limitations of the actual wind tunnel, the Mach range is situated between 0.2 and 0.4. The differences in the air data values for both wind tunnels are considered in the XFoil code simulations. In fact, the results expressed in terms of pressure coefficient distributions versus the chord in XFoil were found to be the same as the results obtained experimentally in the transonic wind tunnel. In the work here presented, we compare only the results obtained with XFoil with results obtained with the MATLAB interpolation programs.

III. Theoretical Considerations

The results obtained by wind-tunnel tests were also obtained by use of the XFoil code, which uses the e^N method for transition point detection coupled with a viscous/inviscid flow panel-method solver [8,9]. The N_{crit} number introduced into the XFoil code was calculated using Mack's correlation [8] using the wind-tunnel freestream turbulence level τ:

$$N_{\text{crit}} = -8.43\text{–}2.4\,\ell n\,\tau \tag{1}$$

In Fig. 2, the pressure coefficients distribution and the predicted transition point are shown for the NACA 4415 airfoil.

It was observed that the transition occurs when there is an increase of the pressure in the boundary layer, which is clearly visible in the C_p plots generated by XFoil code. The increase of pressure was explained by Galbraith and Coton [10] as a separation bubble which appeared in the boundary layer. This separation bubble occurred at low Reynolds numbers and was studied in detail by Arena, O'Meara, and Mueller [4,7].

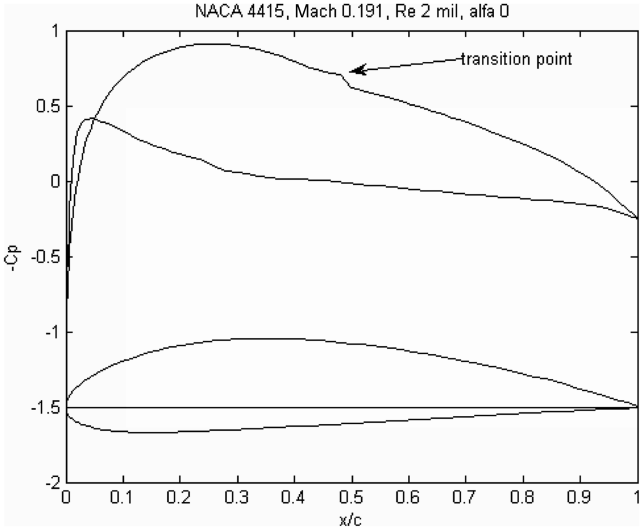

Fig. 2 Pressure distribution and XFoil predicted transition point on the NACA 4415 airfoil at $M = 0.191$, $Re = 2 \times 10^6$, and $\alpha = 0$ deg.

In the low Reynolds number range, an adverse-pressure gradient in the leading-edge flow causes the laminar boundary layer to separate, forming a free shear layer, which, for slightly higher Reynolds number, subsequently undergoes transition to turbulence, and culminates with the incipient reattachment of the turbulent shear layer. This region, delimited upstream and downstream by the laminar separation and turbulent reattachment points is termed a laminar separation bubble. A further increase in Reynolds number, in the medium to high Reynolds number range (5×10^5 to 10^7), promotes transition in the free shear layer causing the reattachment point to migrate toward the leading edge forming a shortened bubble. The laminar flow separation, transition, and turbulent reattachment occur over a small percentage of the chord and are followed by an attached turbulent boundary layer. Eventually, a sufficiently high enough Reynolds number caused the laminar boundary layer to undergo transition before separation so that the bubble disappeared. This phenomenon is typical for most large transport aircraft, for which the Reynolds numbers based on the wing chord are on the order of 10^7 [10].

In the case of our research project, we consider a medium Reynolds number ($2\text{–}4 \times 10^6$) with laminar boundary layers in the flow. However, the laminar boundary layer is very sensitive to adverse-pressure gradients and tends to separate much earlier than a turbulent boundary layer. Thus, in a typical aerodynamic context with a changeover from favorable to adverse-pressure gradient, a region of laminar flow typically ends with a transitional laminar separation bubble soon after the flow encounters the adverse-pressure gradient according to Rist and Augustin [11]. The basic setup of a laminar separation bubble is sketched in Fig. 3. The laminar boundary layer separates from the wall at a point S, transition to turbulence takes place at T, and the turbulent flow reattaches at R. The latter occurs because of an increased momentum exchange normal to the wall under the action of the larger turbulence eddies. With some oversimplification, the reattachment process can be thought to be due to a turbulent wedge that spreads from a point in the

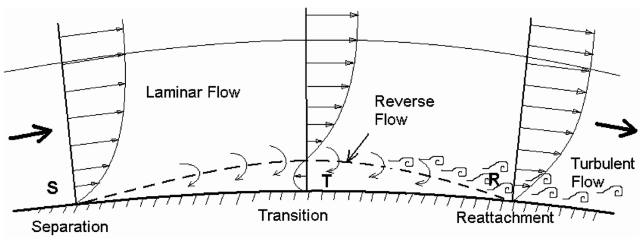

Fig. 3 Schematic of the velocity distributions in the laminar separation bubble.

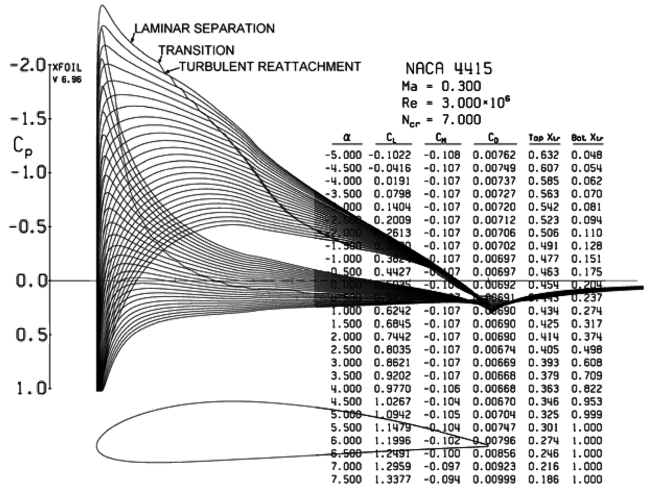

α	C_L	C_M	C_D	Top X_{tr}	Bot X_{tr}
-5.000	-0.1022	-0.108	0.00762	0.632	0.048
-4.500	-0.0416	-0.107	0.00749	0.607	0.054
-4.000	0.0191	-0.107	0.00737	0.585	0.062
-3.500	0.0798	-0.107	0.00727	0.563	0.070
-3.000	0.1404	-0.107	0.00720	0.542	0.081
-2.500	0.2009	-0.107	0.00712	0.523	0.094
-2.000	0.2613	-0.107	0.00706	0.506	0.110
-1.500	[illegible]	-0.107	0.00702	0.491	0.128
-1.000	0.3822	-0.107	0.00697	0.477	0.151
-0.500	0.4427	-0.107	0.00697	0.463	0.175
0.000	[illegible]	-0.107	0.00692	0.454	0.201
0.500	[illegible]	-0.107	0.00691	0.444	0.237
1.000	0.6242	-0.107	0.00690	0.434	0.274
1.500	0.6845	-0.107	0.00690	0.425	0.317
2.000	0.7442	-0.107	0.00690	0.414	0.374
2.500	0.8035	-0.107	0.00674	0.405	0.498
3.000	0.8621	-0.107	0.00669	0.393	0.608
3.500	0.9202	-0.107	0.00668	0.379	0.709
4.000	0.9770	-0.106	0.00668	0.363	0.822
4.500	1.0267	-0.104	0.00670	0.346	0.953
5.000	1.0942	-0.105	0.00704	0.325	0.999
5.500	1.1479	-0.104	0.00747	0.301	1.000
6.000	1.1996	-0.102	0.00796	0.274	1.000
6.500	1.2491	-0.100	0.00856	0.246	1.000
7.000	1.2959	-0.097	0.00923	0.216	1.000
7.500	1.3377	-0.094	0.00999	0.186	1.000

Fig. 4 C_p distributions on a NACA 4415 airfoil at $M = 0.3$ and $Re = 3 \times 10^6$, obtained using the XFoil code.

detached shear layer. The actual transition process starts by amplification of small-amplitude disturbances, which are already present in the upstream laminar flow or which are ingested from the freestream via a process called "receptivity." Once large enough, higher frequencies occur and the shear layer disintegrates into structures of different size [11]. For a detailed study of transition prediction using numerical computational methods and simulations of the laminar separation bubble in low Reynolds number flows, please refer to the paper of Mamou et al. [12].

The laminar-to-turbulent transition point is defined somewhere between the laminar separation and the turbulent reattachment points. Several semi-empirical methods have been developed to determine the transition point location; the most commonly used is the e^n method, which is implemented in XFoil code [8]. Based on experimental observations and linearized stability theory, this method indicates transition when the amplification ratio of any small disturbance in the laminar boundary layer reaches an amplification factor e^n [9]. Figure 4 shows pressure coefficient distributions obtained using the XFoil code for a NACA 4415 reference airfoil at $M = 0.3$, $Re = 3 \times 10^6$, and a range of angles of attack, where the correspondent laminar separation, transition, and turbulent reattachment points are shown in the C_p plots.

The transition point position can be detected in Fig. 3 as the point characterized by a high gradient in the local pressure, which can be explained with the following boundary equation of motion [4]:

$$\rho\left(\frac{\partial u}{\partial t} + u\frac{\partial u}{\partial x} + v\frac{\partial u}{\partial y}\right) = -\frac{\partial p}{\partial x} + \frac{\partial}{\partial y}\left(\mu\frac{\partial u}{\partial y}\right) \tag{2}$$

The viscosity of the fluid imposes the "no-slip condition" at the airfoil surface, that is, $u = v = 0$ at $y = 0$, thus, the flow Eq. (1) reduces to

$$\mu\left(\frac{\partial^2 u}{\partial y^2}\right)_{y=0} = \frac{\partial p}{\partial x} \tag{3}$$

When the pressure gradient is positive, the flow decelerates until it becomes reversed flow. Immediately downstream of the separation point, identified when $(\partial u/\partial y)_{y=0} = 0$, the schematic streamlines near the surface in Fig. 3 show a strong curvature, which is associated with a strong pressure gradient normal to the surface. The streamlines may deflect back toward the surface to form a turbulent boundary layer, or they may deflect further away to form a highly unsteady turbulent shear layer.

The laminar-to-turbulent transition point is defined somewhere between the laminar separation and the turbulent reattachment points. Several semi-empirical methods have been developed to determine the transition point location, the most commonly used is the e^9 method, which is implemented in XFoil code [8]. Based on

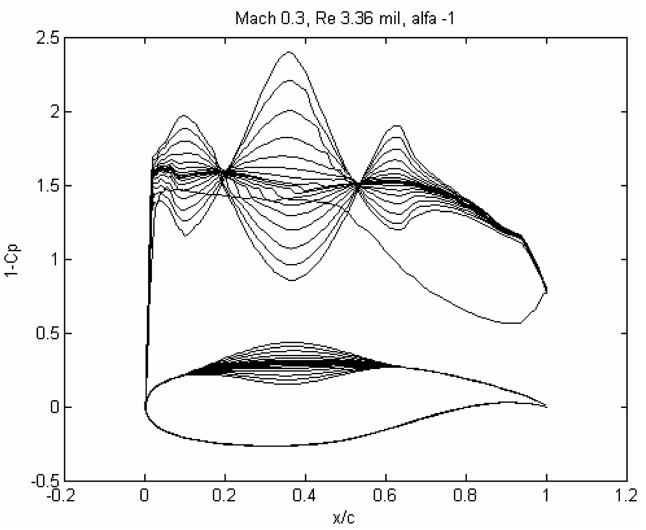

Fig. 5 C_p distributions that correspond to a WTEA-TE1 reference airfoil and to its modified shapes using a single control point, which creates a bump or depression on the airfoil.

experimental observations and linearized stability theory, this method indicates transition when the amplification ratio of any small disturbance in the laminar boundary layer reaches an amplification factor $e^9 \cong 8100$ [9].

The method proposed in this paper is based on the transition point position, defined as the point where the velocity streamline curvature $(\partial^2 u/\partial y^2)_{y=0}$ is maximal along x, which corresponds to its first derivative with x. To obtain this maximum derivative $\partial/\partial x(\partial^2 u/\partial y^2)_{y=0}$, we derive Eq. (2) with respect to x and then we obtain Eq. (4), from which we can see that this first derivative corresponds to the second pressure derivative with respect to x, which should be a maximum:

$$\mu\frac{\partial}{\partial x}\left(\frac{\partial^2 u}{\partial y^2}\right)_{y=0} = \frac{\partial^2 p}{\partial x^2} \tag{4}$$

The maximum in the second derivative of the pressure corresponds to the maximum curvature of the pressure plot, which is associated with the beginning of transition.

A CFD database used by the controller, as described above, was constructed with the aid of the XFoil CFD solver for various flow conditions. This database consists of a collection of airfoil wing

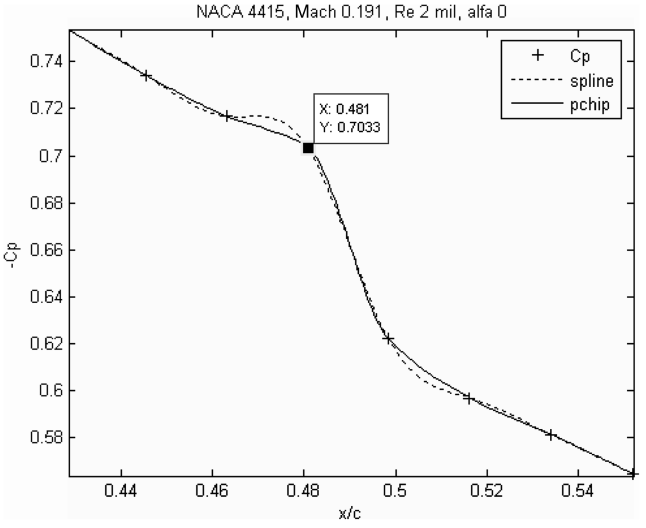

Fig. 6 C_p distributions in the vicinity of the transition point interpolated using the Spline and PCHIP methods.

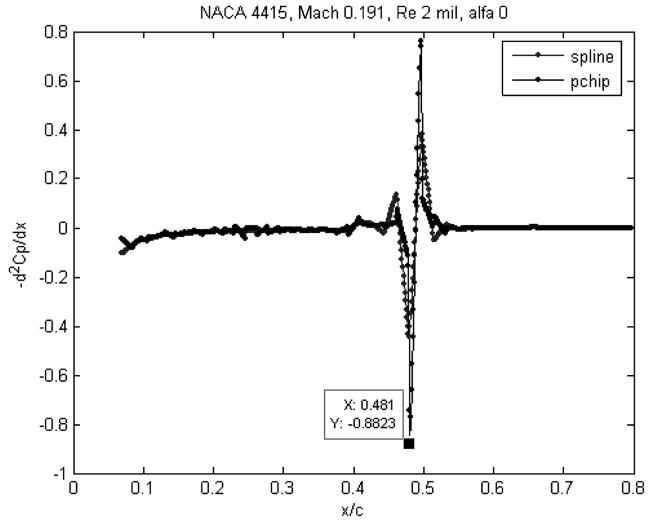

Fig. 7 Second derivative of the C_p distribution interpolated using the Spline and PCHIP methods.

shapes, along with their corresponding pressure coefficient (C_p) versus chord distributions and location of the transition point.

Figure 5 shows the CFD database with several pressure coefficient distributions for the reference WTEA-TE1 airfoil shape (16% thick supercritical airfoil with 68% of the chord in a laminar flow state optimized for transonic speed) and its modified airfoils. The reference airfoil is modified (up and down on the upper airfoil surface) through the use of a single control point (which corresponds to the actuator position) located at 36% of its chord; and thus 16 new modified airfoils with positive and negative deflections of the original airfoil upper surface are obtained.

IV. Results Obtained for a NACA 4415 Airfoil

In this section, the results obtained for the reference NACA 4415 airfoil are presented. The XFoil code is used to simulate the airfoil behavior at a speed of 65 m/s, corresponding to $M = 0.191$ and $Re = 2 \times 10^6$ at a temperature $T = 15°C$ with a chord of 0.4572 m (1.5 ft). To determine the curvature (second derivative) of the C_p distribution, two interpolation methods are used: Spline and PCHIP (piecewise cubic Hermite interpolating polynomial) [13]. The PCHIP method finds the values of an underlying interpolating

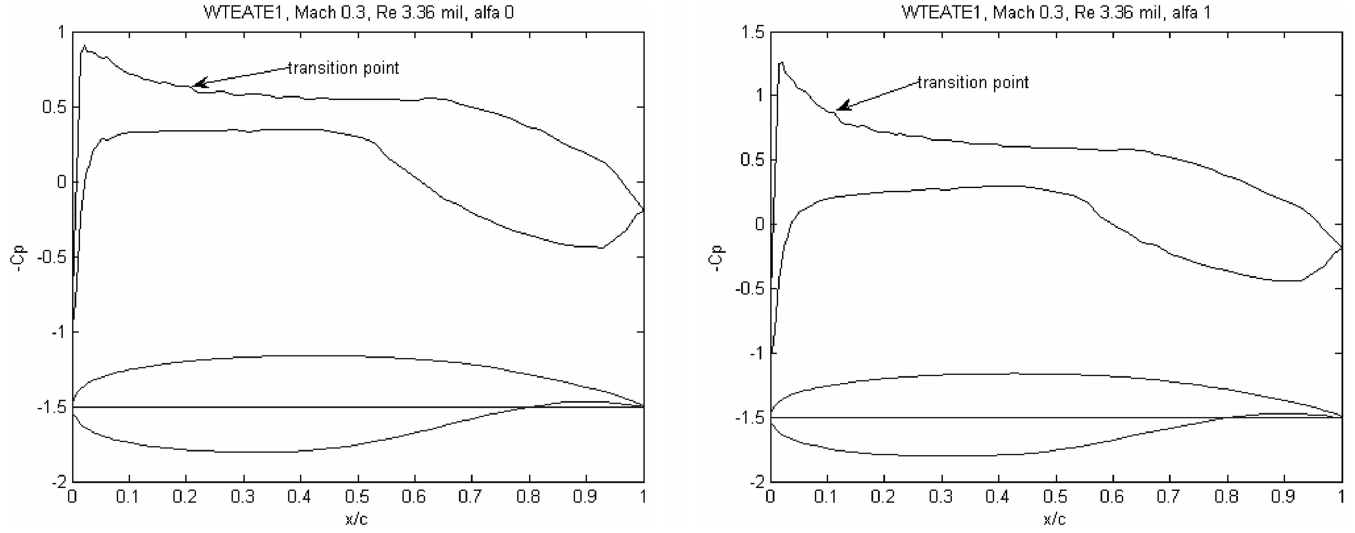

a) b)

Fig. 8 C_p distributions on the upper and lower surface of the WTEA-TE1 airfoil at a) $\alpha = 0$ deg and at b) $\alpha = 1$ deg.

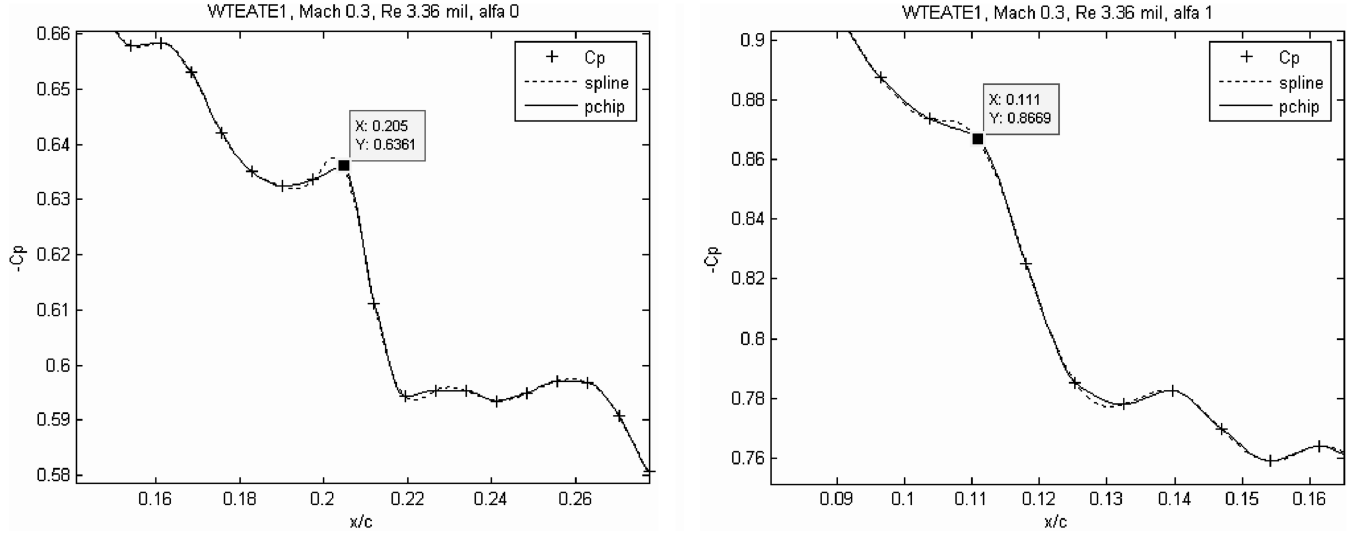

a) b)

Fig. 9 $C_p(x)$ at a) $\alpha = 0$ deg and at b) $\alpha = 1$ deg by use of Spline and PCHIP methods.

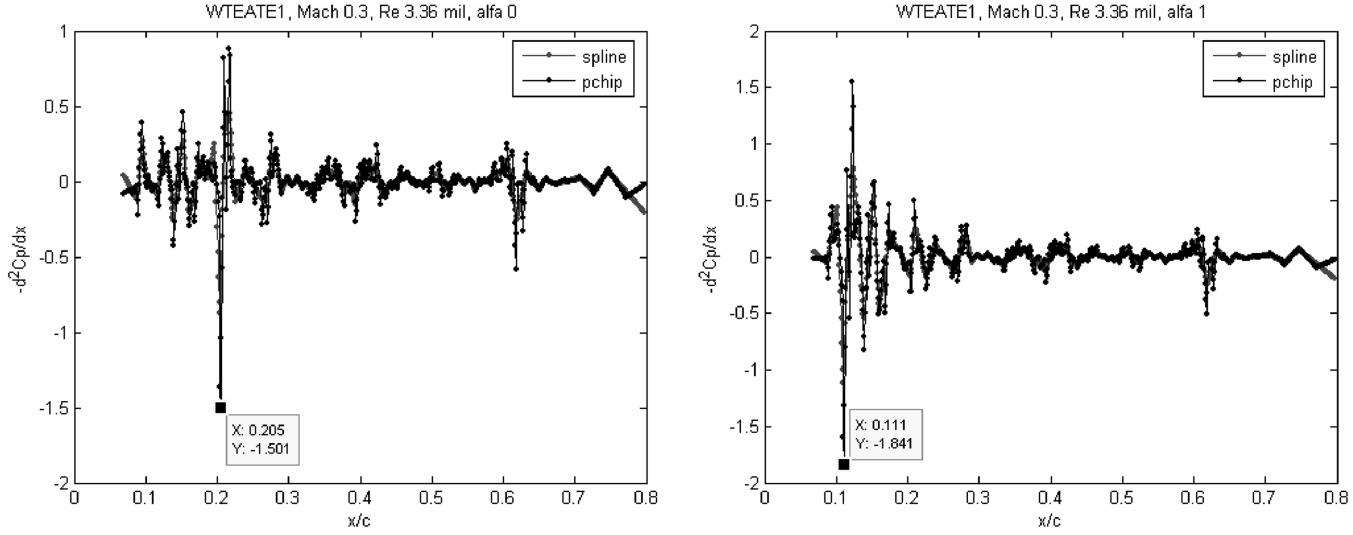

a) b)

Fig. 10 Second derivative of C_p at a) $\alpha = 0$ deg and at b) $\alpha = 1$ deg by use of Spline and PCHIP methods.

function $p(x)$ at intermediate points, such that on each subinterval $x_k \leq x \leq x_{k+1}$, $p(x)$ is the cubic Hermite interpolant to the given values and their slopes at the two endpoints x_k and x_{k+1}. The function $p(x)$ interpolates between the points values, and its first derivative $p'(x)$ is continuous. The second derivative $p''(x)$ may be discontinuous, as there might be jumps in the x_k points. The slopes at these points are chosen in such a way that $p(x)$ preserves the data shape and respects its monotonicity, which is to say that on the interval in which the data is monotonic or has a local extreme, the same interval $p(x)$ is monotonic or has a local extreme. The Spline method constructs the interpolation polynomial in almost the same manner as the PCHIP. With Spline, the slopes at the x_k points are chosen differently, so that the second derivative should be continuous, which results in a smoother result. The Spline method produces a more accurate result if the data consist of smooth function values while the PCHIP method has no overshoots and less oscillation if the data are not smooth, an advantage for the pressure distribution interpolations in the vicinity of the transition point, characterized by a sudden pressure increase.

Figure 6 which displays the C_p distribution interpolated in the vicinity of the transition point using both the Spline and the PCHIP methods, clearly indicates that the step in the pressure at the point of transition is more accurately interpolated by the PCHIP method than by the Spline function. Figure 7, which illustrates the second derivative of the C_p distribution, shows the maximum value of the C_p second derivative (equivalent to the minimum value of the negative C_p second derivative) determined from both methods of interpolation. The locations of transition determined under these conditions from the PCHIP and Spline interpolation methods are within 0.06 and 0.04% of the airfoil chord, respectively, compared to the transition position obtained directly from the XFoil code, suggesting a fairly high accuracy in the determination of the transition point.

V. Results Obtained for the WTEA-TE1 Airfoil

The two interpolation methods presented above were applied to a set of 17 airfoil shapes derived through modifications to the reference WTEA-TE1 airfoil (the notation TE1 stands for an airfoil configuration with a blunt trailing edge). The simulation conditions are $M = 0.3$, $Re = 3.36 \times 10^6$, and temperature $= 15°$C. The values of airfoil deflections at the control point here considered are $= \pm 20$, ± 16, ± 12, ± 8, ± 5, ± 3, ± 1.5, ± 0.5, and 0 mm, while the airfoil chord was equal to 0.5 m. The angle of attack was set to various values: -2, -1, 0, 1, and 2 deg. Therefore, a total of 85 cases (5 angles of attack multiplied by 17 airfoil deflections) was obtained for which the transition point position was calculated.

The WTEA-TE1 airfoil surface pressure coefficients calculated with the XFoil code are presented in Figs. 8 for two angles of attack $\alpha = 0$ deg and $\alpha = 1$ deg. Figures 9 and 10 show the pressure coefficient distributions $C_p(x)$ and second derivatives versus the airfoil chord obtained for two angles of attack $\alpha = 0$ deg and $\alpha = 1$ deg by both interpolation methods, Spline and PCHIP. The location of transition predicted by XFoil was found to be 0.2040, respectively, 0.1118, and based on the maximum pressure curvature criterion, is also identified in Figs. 9 and 10. The error associated with the determination of the transition point, relative to the theoretically determined value identified in Fig. 10, was $0.1\%c$ at $\alpha = 0$ deg and below $0.1\%c$ at $\alpha = 1$ deg.

Tables 1 and 2 show the relative errors of the transition point positions, as a fraction of the airfoil chord, calculated by the PCHIP method versus XFoil code (Table 1) and by the Spline method versus XFoil code (Table 2) obtained for the two reference wing airfoils, NACA 4415 and WTEA-TE1, and for the 17 modified airfoils of the WTEA-TE1 for five angles of attack. The total mean error calculated with the PCHIP method versus XFoil code was found, from Table 1,

Table 1 The relative errors, as a fraction of the airfoil chord, for the transition point prediction calculated by the PCHIP versus the XFoil method

PCHIP method	−2 deg	−1 deg	0 deg	1 deg	2 deg
NACA 4415	0.0061	0.0057	0.0006	0.0051	**0.0092**
WTEA-TE1	0.0030	0.0003	0.001	0.0008	**0.0038**
20.0 mm	0.0017	0.0008	0.0003	0.0007	0.0019
16.0 mm	0.0016	0.0053	0.0003	0.0035	0.0042
12.0 mm	0.0027	0.0017	0.0011	0.0006	0.0009
8.0 mm	0.0014	0.0007	0.0006	0.0016	0.0026
5.0 mm	0.0010	0.0002	0.0044	0.0035	0.0001
3.0 mm	0.0014	0.0019	0.0031	0.0018	0.0002
1.5 mm	0.0018	0.0058	0.0052	0.0037	0.0023
0.5 mm	0.0054	0.0051	0.0029	0.0013	0.0032
0 mm	**0.0091**	0.0053	0.0015	0.0000	0.0006
−0.5 mm	0.0042	0.0037	0.0041	0.0014	0.0017
−1.5 mm	0.0044	0.0016	0.001	0.0053	0.0005
−3.0 mm	0.0014	0.0022	0.0014	0.0019	0.0033
−5.0 mm	0.0027	0.0022	0.0003	0.0006	0.0006
−8.0 mm	0.0030	0.0032	0.0001	0.0001	0.004
−12.0 mm	0.0029	0.0003	0.0002	0.0006	0.002
−16.0 mm	0.0028	0.0039	0.0025	0.0008	0.0007
−20.0 mm	0.0019	0.0011	0.0024	0.0026	0.0014
Mean error	0.0031	0.0027	0.0017	0.0019	0.0023

Table 2 The relative errors, as a fraction of the airfoil chord, for the transition point prediction with the Spline versus the XFoil method

Spline method	−2 deg	−1 deg	0 deg	1 deg	2 deg
NACA 4415	0.0051	0.0047	0.0004	0.0041	**0.0102**
WTEA	**0.0740**	0.0003	0.0000	0.0018	0.0082
20.0 mm	0.0007	0.0018	0.0087	0.0003	0.0009
16.0 mm	0.0026	0.0033	0.0007	0.0045	0.0032
12.0 mm	0.0037	0.0007	0.0021	0.0016	0.0019
8.0 mm	0.0004	0.0007	0.0016	0.0194	0.0006
5.0 mm	0.0000	0.0008	0.0034	0.0145	0.0011
3.0 mm	0.0014	0.0009	0.0021	0.0008	0.0012
1.5 mm	0.0008	0.0048	0.0042	0.0027	0.0033
0.5 mm	0.0044	0.0041	0.0019	0.0023	0.0012
0 mm	**0.0071**	0.0007	0.0005	0.0010	0.0004
−0.5 mm	0.0032	0.0027	0.0031	0.0014	0.0007
−1.5 mm	0.0054	0.0016	0.0020	0.0033	0.0005
−3.0 mm	0.0004	0.0012	0.0004	0.0019	0.0033
−5.0 mm	0.0017	0.0032	0.0007	0.0016	0.0004
−8.0 mm	0.0020	0.0022	0.0009	0.0009	0.0030
−12.0 mm	0.0039	0.0013	0.0008	0.0004	0.0020
−16.0 mm	0.0038	0.0039	0.0015	0.0008	0.0003
−20.0 mm	0.0029	0.0001	0.0034	0.0026	0.0004
Mean error	0.0065	0.0021	0.0020	0.0035	0.0023

to be 0.23%c and the total mean error calculated with the Spline method versus XFoil code was found, from Table 2, to be 0.33%c, from which it can be concluded that the PCHIP method gives better results in this application. The maximum errors are shown in Tables 1 and 2 in bold figures. Note that the WTEA-TE1 has a different shape than the 0-mm displacement airfoil because for the latter spline curves were used to define the upper surface between 0.07 and 0.65 x/c.

The precision with which the location of the transition point is determined is dictated by the density of the pressure sensors distributed along the airfoil chord. In the current investigation, the XFoil software is used to simulate the C_p distribution at 84 and 37 points for the WTEA and NACA 4415 airfoils, respectively, within the 7–65% chord interval, where a flexible skin should be equipped with smart actuators. For both the NACA 4415 and WTEA airfoils considered in this paper, the location of the transition point as a function of the pressure coefficient distribution was determined with a high precision of 0.1% of a chord between 7 and 80% of the chord, given the current measurement resolution.

VI. Conclusions

A method for the detection of the location of laminar-to-turbulent transition on the suction surface of an airfoil from the surface pressure distribution was examined. It was found, through validation using the XFoil code, that the transition point may be identified via the maximum curvature of the surface pressure distribution. This technique identified the location of the transition point with a mean accuracy of 0.23 or 0.33% of the airfoil chord, depending on whether the PCHIP or Spline interpolation method was implemented. This method does not, however, replace the theoretical e^N method or other boundary-layer numerical methods. Indeed, it is based on the results obtained by these methods, expressed in terms of pressure coefficient distribution versus the airfoil chord.

This method is advantageous in its real-time applicability, such as in the controller of a morphing wing model, which would measure the pressure distribution, compute the second derivative, and then identify the position of transition to be used as the indicator on how to modify the wing shape. There are limitations, however, to this method related to the range in which the transition point can be located; the method does not work well in the vicinity of the leading-edge suction peak, necessitating its elimination. In addition, accurate determination of the location of the transition point is dependent on a sufficient density of pressure measurements along the airfoil chord.

Future work will involve experimental verification of the theoretically based results presented above. The effect of transition point position on the wing drag reduction will be determined, and, in this way, a controller to modify in real time the airfoil geometry will be developed.

Acknowledgments

We would like to thank CRIAQ (Consortium of Research in the Aerospace Industry in Quebec), Bombardier Aerospace, Thales Avionics, the NRC-IAR (National Research Council—Institute for Aeronautical Research), and the NSERC (National Sciences and Engineering Research Council) for the funds which made this research possible. We would also like to thank Bombardier Aerospace, Thales Avionics, and NRC-IAR for their collaboration in this work.

References

[1] Jacob, J. D., "On the Fluid Dynamics of Adaptive Airfoils," *Proceedings of 1998 ASME International Mechanical Engineering Congress and Exposition*, ASME, Fairfield, NJ, Nov. 1998, pp. 167–176.

[2] Driver, J., and Zingg, D. W., "Optimized Natural-Laminar-Flow Airfoils," AIAA Paper 2006-0247, Jan. 2006.

[3] Zingg, D. W., Diosady, L., and Billing, L., "Adaptive Airfoils for Drag Reduction at Transonic Speeds," AIAA Paper 2006-3656, June 2006.

[4] Arena, A. V., and Mueller, T. J., "Laminar Separation, Transition, and Turbulent Reattachment Near the Leading Edge of Airfoils," *AIAA Journal*, Vol. 18, No. 7, 1980, pp. 747–753.

[5] Khrabrov, A., and Oi, M. V., "Effects of Flow Separation on Aerodynamic Loads in Linearized Thin Airfoil Theory," *Journal of Aircraft*, Vol. 41, No. 4, 2004, pp. 944–948.

[6] Khabrov, A., and Greenwell, D., "Influence of Steady Pitch Rate on 2-D Airfoil Aerodynamic Characteristics at Incidence," *Journal of Aircraft*, Vol. 43, No. 5, 2006, pp. 1552–1555. doi:10.2514/1.19198

[7] O'Meara, M. M., and Mueller, T. J., "Laminar Separation Bubble Characteristics on an Airfoil at Low Reynolds Numbers," *AIAA Journal*, Vol. 25, No. 8, 1987, pp. 1033–1041.

[8] Drela, M., "Implicit Implementation of the Full e^n Transition Criterion," AIAA Paper 2003-4066, 2003.

[9] Drela, M., and Giles, M. B., "Viscous-Inviscid Analysis of Transonic and Low Reynolds Number Airfoils," *AIAA Journal*, Vol. 25, No. 10, 1987, pp. 1347–1355.

[10] Galbraith, R. A., and Coton, F. N., "Two-Dimensional, Incompressible Aerofoil Design and Analysis," *Computational Methods in Viscous Aerodynamics*, edited by T. K. S. Murthy and C. A. Brebbia, Computational Mechanics Publications, Ashurst Lodge, Southampton, U.K., 1990, pp. 331–367.

[11] Rist, U., and Augustin, K., "Control of Laminar Separation Bubbles Using Instability Waves," *AIAA Journal*, Vol. 44, No. 10, 2006, pp. 2217–2223. doi:10.2514/1.17518

[12] Mamou, M., Yuan, W., and Khalid, M., "Transition Prediction in Low Reynolds Airfoil Flows Using Finite Element/Difference Solvers Coupled with the e^n Method: A Comparative Study," AIAA Paper 2006-3176, June 2006.

[13] Fritsch, F. N., and Carlson, R. E., "Monotone Piecewise Cubic Interpolation," *SIAM Journal on Numerical Analysis*, Vol. 17, No. 2, 1980, pp. 238–246. doi:10.1137/0717021